A neuromorphic bionic eye with broadband vision and biocompatibility using TIPS-pentacene-based phototransistor array retina

Haizhong Zhang[1§*], Xin Ju[2§*], Dongzhi Chi[2], Linrun Feng[3], Zhe Liu[3], Kwangsing Yew[4], Minmin Zhu[1], Tiaoyang Li[1], Rongshan Wei[1], Shaohao Wang[1], Linfeng Sun[5], Zhongrui Wang[6], and Yanqing Wu[7]

[1]College of Physics and Information Engineering, Fuzhou University, Fuzhou, China, 350116;
[2]Institute of Materials Research and Engineering, Agency for Science, Technology and Research, 2 Fusionopolis Way, Singapore, 138634;
[3]LinkZill Technology Co., Ltd., Hangzhou, Zhejiang, China, 310000;
[4]GlobalFoundries, 60 Woodlands Industrial Park D Street 2, Singapore, 738406;
[5]School of Physics, Beijing Institute of Technology, Beijing, China, 100081;
[6]Department of Electrical and Electronic Engineering, The University of Hong Kong, Pokfulam Road, Hong Kong;
[7]Institute of Microelectronics, Peking University, Beijing, China, 100871;
[*]Corresponding authors:
Emails: haizhong_zhang@fzu.edu.cn; ju_xin@imre.a-star.edu.sg
[§]Equal contribution to this work

Keywords*:* optoelectronic neuronic device; bionic eyes; broadband vision; all-organic phototransistor; TIPS-pentacene;

ABSTRACT

Taking inspiration from the human eye's information processing capabilities, the artificial optoelectronic neuronic device (AOEND) offers a promising approach to creating a bionic eye that performs real-time, low-power processing by integrating optical sensors, signal processing, and electronic neurons into a single device. Despite significant advancements, the current AOEND still faces challenges in terms of power consumption, flexibility, bio-compatibility, and, most importantly, achieving photo-sensitivity across the same broadband perceivable wavelength range (380 nm to 740 nm) as the human eye. In this study, we present a commercially ready, dual-gated thin-film-transistor (TFT)-based AOEND. Our device exhibits exceptional photo-response to specific wavelengths by utilizing an organic TIPS-pentacene material as the channel layer and intentionally tailoring its optical bandgap to approximately 1.6 eV. Additionally, the device successfully replicates various photon-triggered synaptic characteristics and performs visual sensing, memory processing, and other functions with low power consumption. Our findings present a viable strategy for the development of future integrated sensing-memory-processing flexible devices for optoelectronic artificial retina perception applications.

1. Introduction

Artificial intelligence (AI) systems are more ubiquitous than ever, exerting influence over nearly every aspect of modern civilized life. These systems encompass a wide range of applications, including smart sensing, facial recognition, image or pattern classification, natural language processing, autonomous cars, robotics, healthcare, and smart cities, among others.[1-9] In this pursuit, the integration and deployment of AI and Internet of Things (IoT)-enabled solutions heavily rely on sensors, memories, and processors. These components serve as nodes that perceive, store, and convert physical world information into digital data. One particular area of interest lies in the development of new visual sensors inspired by the human eye. Such sensors have the potential to assist visually impaired individuals and offer machines advanced perception capabilities. However, the majority of bionic eyes currently in development are based on machine vision systems, which lack the dexterity and intelligence of the human eye. These systems typically consist of two separate modules: an external camera module for image capturing and an implanted image processor module for image sampling, processing, and storage. The complex circuitry, lengthy response time, high power consumption, and bulky design of prosthetic eyes are inherent issues arising from the extensive analog-to-digital conversion and data transfer required between physically separated photoreceptors, memory, and processing units. These limitations hinder the widespread adoption of prosthetic eyes, particularly in time-sensitive and power-constrained scenarios.

In contrast, the human vision system, as depicted in **Figure** 1a, can efficiently perceive complex environmental information while consuming ultra-low power. The eye bulbs, a critical component of the optical perception intelligence function, enable the acquisition of external optical stimuli through photoreceptors, optic rods, and cone cells. The sensory neuroelectric signals are processed via the release of various excitatory and inhibitory neurotransmitters by internal neurons. Millions of nerve fibers are responsible for data transmission, and in conjunction with the human cerebral cortex, they possess an extensive parallel data processing capacity for precise learning. Artificial optoelectronic neuronic devices (AOENDs) with biological synaptic functions are considered crucial for the development of future bionic eyes, as they

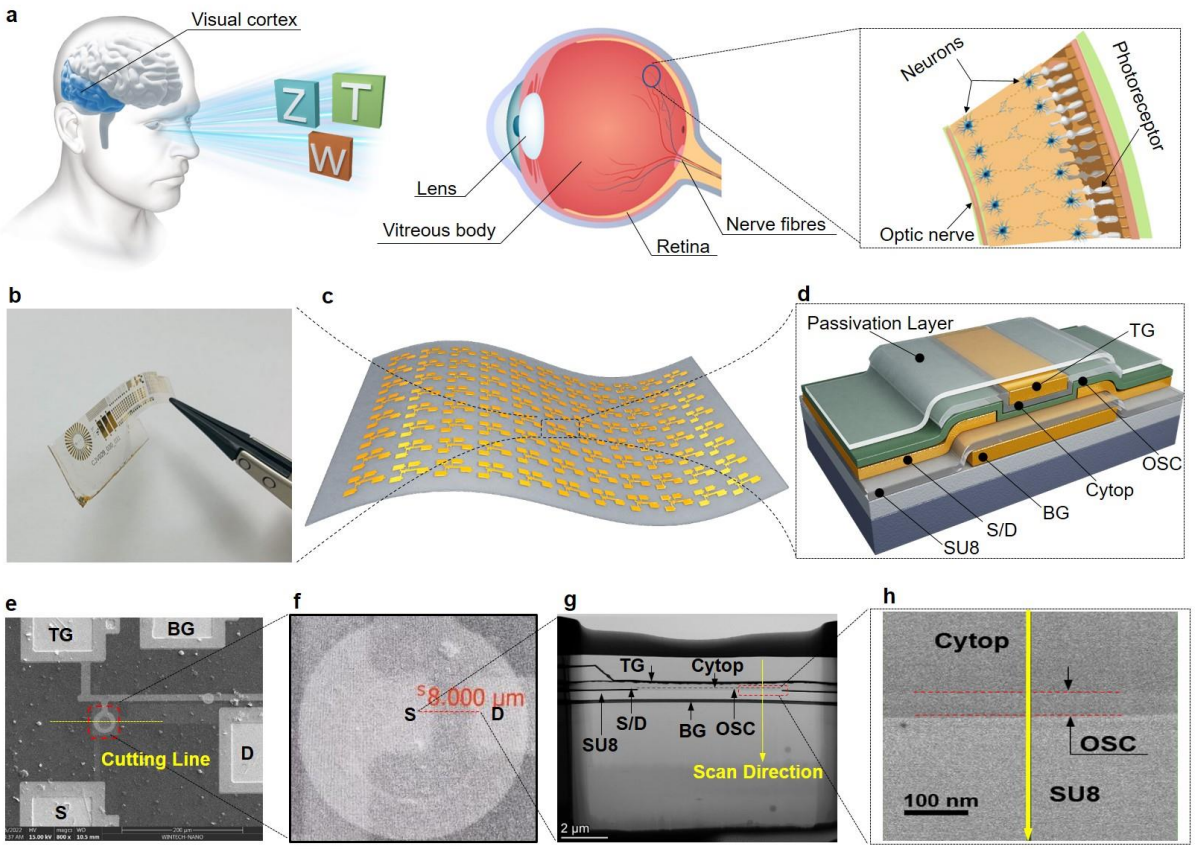

Figure 1. (a) Schematic illustrations of human visual perception systems, especially the detailed eye bulb, and retinal structure. The role of neurons is to transmit light-dependent signals to the visual cortex. (b) The original photograph of a conformal device array, demonstrating the stretchable and curlable properties. (c) The schematic diagram of fabricated stretchable and curlable device array. (d) The schematic diagram of our dual-gated TFT-based optoelectronic neuromorphic device. "TG", "BG", "S" and "D" represent the top gate, bottom gate, source and drain electrodes, respectively. Optical microscopy image of the full optoelectronic neuronic component in a fabricated array. (e, f) Scanning electron microscope (SEM) image of a top view of the whole dual-gated TFT device and focused source/drain area. (g, h) High-resolution cross-sectional transmission electron microscopy (HRTEM) images of the active area and zoom-in of the channel layer, respectively. The red dashed box and yellow line indicate the area and direction of the energy dispersive X-ray (EDX) mapping analysis.

eliminate the need for an external camera and processor, allowing to emulate the functionality of natural eyes. Building upon this premise, the invention of electro- and photo-sensitive bionic eyes emerged as a promising solution, enabling direct response to optical signals, and combining functions such as image acquisition, data processing, and signal transmission in a synergistic manner. This approach offers several advantages, including a compact design, reduced power consumption, and a decreased number of logic operations.[10-15]

Over the past years, hybrid electro-photonic devices utilizing a range of materials, such as metal oxides,[16-18] Si nanocrystals,[19] perovskites,[20,21] and two-dimensional (2D) materials,[12-14, 22-24] have gained significant attention. These devices, which rely on two-terminal memristors and three- (four-/multi-) terminal field-effect transistors (FETs), have been extensively explored to achieve photoelectric synaptic plasticity, allowing them to respond to varying light conditions. Moreover, these devices offer the advantages of high bandwidth, low latency, low power consumption, and efficient information processing, thereby bridging the gap between brain computing and optical sensing. Despite notable advancements in the field, the practical implementation of photo-responsive devices for bionic eyes remains challenging due to limited functionality and poor reliability. Notably, the IGZO material, facilitated by the mature production of IGZO-based thin-film transistors (TFTs), stands out as a promising candidate for electro-photo-sensitive artificial synaptic applications. However, its relatively large optical bandgap of approximately 3.05 eV restricts its photo-sensitivity to the ultraviolet (UV) spectrum, and it cannot cover the entire visible range through direct light excitation.[17,18] While defect states within the bandgap may enhance photo-response, they can compromise the device's reliability and repeatability. Certain 2D materials-based AOENDs exhibit favorable photoelectric responses to visible light, but challenges such as process maturity, reproducibility, stability, and uniformity of 2D materials persist.[11-14] Additionally, most existing photo-responsive devices rely on rigid substrates, limiting their application in flexible integration platforms and hindering their use in wearable and implantable electronics. In contrast, organic semiconductors offer a new approach by serving as active materials for electrical transport and photon absorption, mimicking biological photoreceptors due to their unique optoelectronic properties. Furthermore, organic materials exhibit superior biocompatibility for cellular photo-stimulation, allowing for the realization of artificial retinas through tissue integration. However, research on organic-based AOENDs remains limited at present.[25,26]

In this study, we present a comprehensive investigation of highly reliable, low-power, and fully flexible electro-photo-sensitive neuronic units. We achieve this by employing an all-organic dual-gated TFT with commercial production

capability (refer to **Figures** 1b and 1c). Resultantly, the photo-responsive device utilizes TIPS-pentacene as the organic semiconductor channel layer due to its commercial fabrication readiness, stability, flexibility, biocompatibility,[27] and most importantly, its feature of a small tunable optical bandgap of approximately 1.6 eV.[28] This characteristic is particularly advantageous for the implementation of bionic eyes. TIPS-pentacene-based photo-responsive devices exhibit exceptional responsiveness across the entire perceivable wavelength range, enabling them to adapt to a wide variety of scenes at photo-sensory terminals. Moreover, as-fabricated phototransistor array seamlessly integrates information storage and data preprocessing capabilities, allowing for rich dynamic behavior through the co-modulation of light and electrical stimulation. Our opto-neuronal device provides a new strategy for the development of bionic eyes and other artificial neuromorphic vision systems, which will ultimately unlock the advantages associated with visual cognition and memory.

2. Results and discussions

The structure of the dual-gated TFT-based AOEND is visually represented in **Figure** 1d. **Figure**1e illustrates a top view captured by a scanning electron microscope (SEM), showcasing the typical as-fabricated AOEND. Additionally, **Figure**1f zooms in on the source/drain region, allowing for a detailed examination of this crucial area. To ensure the production of high-quality organic layers, the confirmation is provided through **Figures** 1g and 1h. The transmission electron microscope (TEM) image demonstrates the continuous stacking of the gate electrode Au on a flexible PET substrate, the SU-8 bottom gate dielectric, the tailored organic semiconductor (OSC) channel, and the Cytop top gate dielectric. The composition analysis carried out using energy-dispersive X-ray (EDX), further validates the presence of individual elements within the stack, as shown in **Figure** S1. The detailed fabrication process can be found in the Methods section. Presynaptic stimulus is applied to the top gate (electrical signals) and the OSC layer (light illumination). The postsynaptic current is represented by the channel current transmitted between the source and drain (I_{DS}). The device operates in linear mode near the off-current state, with V_{GS} = +18 V and V_{DS} = –2 V, while the bottom gate (V_{BG}) remains floating. **Figure** 2a and **Figure** S2 display the typical output (I_{DS}–V_{DS}) and transfer (I_{DS}–V_{GS}) characteristics of the device,

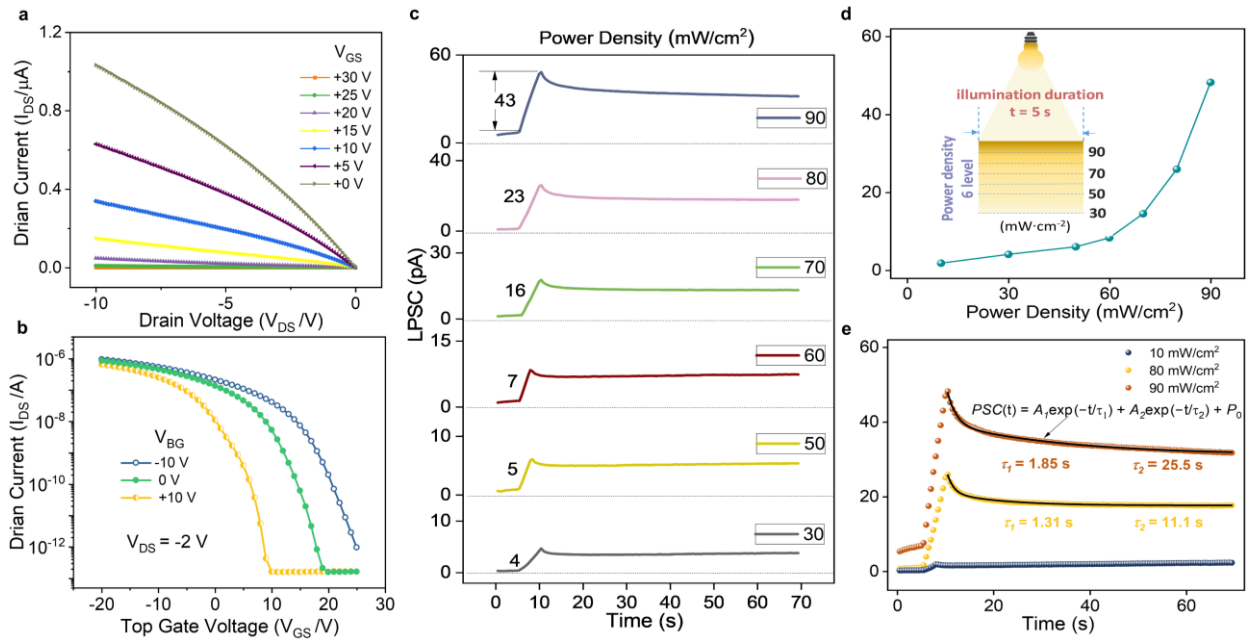

Figure 2. (a) Output characteristics of the dual-gated optoelectronic transistor with V_{DS} sweeping from 0 to –10 V under various V_{TG}. (b) Transfer characteristics of the device with V_{TG} sweeping from +25 to –20 V under three different V_{BG}, thus confirming effective modulation of turn-on voltage by varying V_{BG}. The optoelectronic properties of a double-gated synaptic transistor, in which a controlled optical pulse is generated utilizing a LED light source. (c) Photo-response of the device at different light power intensities, exhibiting a clear change in the current magnitude. (d) Indication of the positive correlation between LPSC and optical power density, LPSC increases as the light intensity increases due to an increase in photo-generated *e-h* pairs. (e) LPSCs of the device triggered by an optical pulse (500 ms), and relaxation time constants in the rapid and slow decay phases.

respectively. The coupling between the bottom gate and the channel is comparatively weaker when compared to the top gate. As a result, the bottom gate is primarily utilized as a control gate in the transistor operation. By sweeping the bias voltage of the top gate (V_{TG}) from +25 to –20 V under three different V_{BG} conditions, a significant shift in the turn-on voltage, from +7 to +1.5 V, is observed, indicating that the threshold voltage (V_{th}) of the device can be precisely modulated by V_{BG} (**Figure** 2b). When a positive V_{BG} is applied, it depletes the p-channel carriers within the channel, leading to a negative shift of the V_{th} in transfer characteristics. Conversely, when a negative V_{BG} is applied, it induces a positive shift of V_{th}, owing to additional hole induction in the channel. We would like to emphasize that an operation voltage in the range of tens of volts may appear relatively high, it is commonly observed in organic TFTs and can be reduced as the device size is scaled down. The device demonstrates a large on/off ratio of ~10^7 and a maximum off-current value of 0.16 pA (from a 3×3 device array), highlighting its low static power consumption advantage. Electrical performance of the

other 8 devices shows 100% functional operation with very small device-to-device variation (**Figure** S3). The intensity of the stimulus plays a crucial role in synaptic plasticity regulation, where weak input signals lead to short-term plasticity resulting in rapid relaxation of the postsynaptic conductance state to the initial conductance state, while strong input signals lead to long-term plasticity resulting in a long-lived steady state. This phenomenon has been well-documented in studies on synaptic plasticity, specifically in the regulation of neuronal responses.[29-31] When the device was exposed to white light, an observable light-induced postsynaptic current (LPSC) was generated, which could be adjusted by varying the illumination power density (**Figure** 2c). It is important to note that the LPSC initially exhibits a rapid increase and then gradually decays to a steady state after the light source is removed. The change in LPSC is defined as the difference between the peak LPSC and the current level observed without illumination. As the illumination power density is increased, a stronger photo-response is observed, indicating that the optical sensing and memory capabilities of our biomimetic visual transistor can be enhanced by amplifying the light intensity. LPSC readings were conducted after ten consecutive light pulses with a pulse width of 0.5 s, as illustrated in **Figure** 2d. Following the cessation of light illumination, the decay characteristics of LPSC corresponding to various light power densities are observed (**Figure** 2e). The results demonstrate that LPSC exhibits a slight increase after illumination with low-intensity light (10 mW·cm^{-2}) and subsequently returns to its initial state after the light pulses cease. In the case of higher light intensities (i.e., 80 mW·cm^{-2} and 90 mW·cm^{-2}), LPSC gradually decays before reaching a steady state. Furthermore, the device maintains a higher conductance state even after optical potentiation. Additionally, LPSC corresponding to 90 mW·cm^{-2} requires a longer time to stabilize compared to that of 80 mW·cm^{-2}. The decay of the retained LPSC can be effectively modeled using a double exponential function, as follows:[32]

$$PSC(t) = P_0 + A_1 \cdot exp\left(-t/\tau_1\right) + A_2 \cdot exp\left(-t/\tau_2\right) \quad (1)$$

where *PSC* (*t*) represents the memory level at time *t*, while P_o denotes the steady state. A_1 and A_2 are the fitting prefactors, and τ_1 and τ_2 represent the time constants associated with the rapid and slow relaxation phases, respectively, which

correspond to the forgetting rate. Specifically, τ_1 is immediately after the light pulse, attributed to the emission of shallow traps within a very short duration. On the other hand, τ_2 characterizes the slow decay, which originates from deep traps with longer emission times until the PSC reaches its steady-state value, P_o. The fitted values for τ_1 and τ_2 are found to be 1.31 s and 11.1 s (1.85 s and 25.5 s) for light intensities of 80 (90) mW·cm^{-2}, respectively. These results indicate an increase in the slow decay time constant τ_2 with the rise in intensity. It is noteworthy that the kinetics of LPSC decay closely resemble the memory loss behavior observed in neuronal systems. Moreover, the photonic response exhibited by the device emulates the potentiation effect observed in visual sense synapses. Consequently, our bionic visual transistor showcases positive retinal traits, aligning with the functionalities observed in biological visual systems.

Our optoelectronic device demonstrates favorable electrical and optical coupling performance, as illustrated in **Figure** 3. The device exhibits characteristic synaptic plasticity with an excitatory postsynaptic current (PSC) that increases in response to an increasing number of pre-synaptic light pulses (30 mW·cm^{-2}, pulse width of 0.5 s, and pulse number of 10) (**Figure** 3a). During this process, the device operates in a four-terminal mode and an off-current state with V_{TGS} = +20 V and V_{DS} = −2 V. Upon light deactivation, the current gradually decays (i.e., forgetting) as discussed earlier, rather than rapidly returning to the initial level, which can be attributed to the inherent persistent photoconductivity effect. The PSC of the device promptly returns to the initial state when a subsequent electrical pulse is applied to the bottom gate (V_{BGS} = −20 V, pulse width of 0.5 s), thus achieving photoelectric tunability through optical potentiation and electrical erase behavior. Following the removal of the electrical pulse, a slight recovery of the current can be observed. Notably, the light-induced potentiation and electrical depression processes exhibit high repeatability. On top of this, the influence of light intensity, as the primary training parameter for synaptic plasticity, is further investigated (**Figure** 3b). It is observed that the PSC progressively increases with the application of consecutive light pulses, followed by a gradual decrease to its initial level with the application of consecutive electrical pulses. An independent electrical erase operation is crucial for initializing and reusing the device. After the electrical pulse trains, the device can be completely reset to either the

initial state or a lower current state, irrespective of the light intensity. These results confirm the effective responsiveness of our device to external photoelectric stimuli, validating a robust and reproducible learning process. This fundamental premise establishes its promising potential for deployment in photonic-electronic-coupled bionic visual networks.

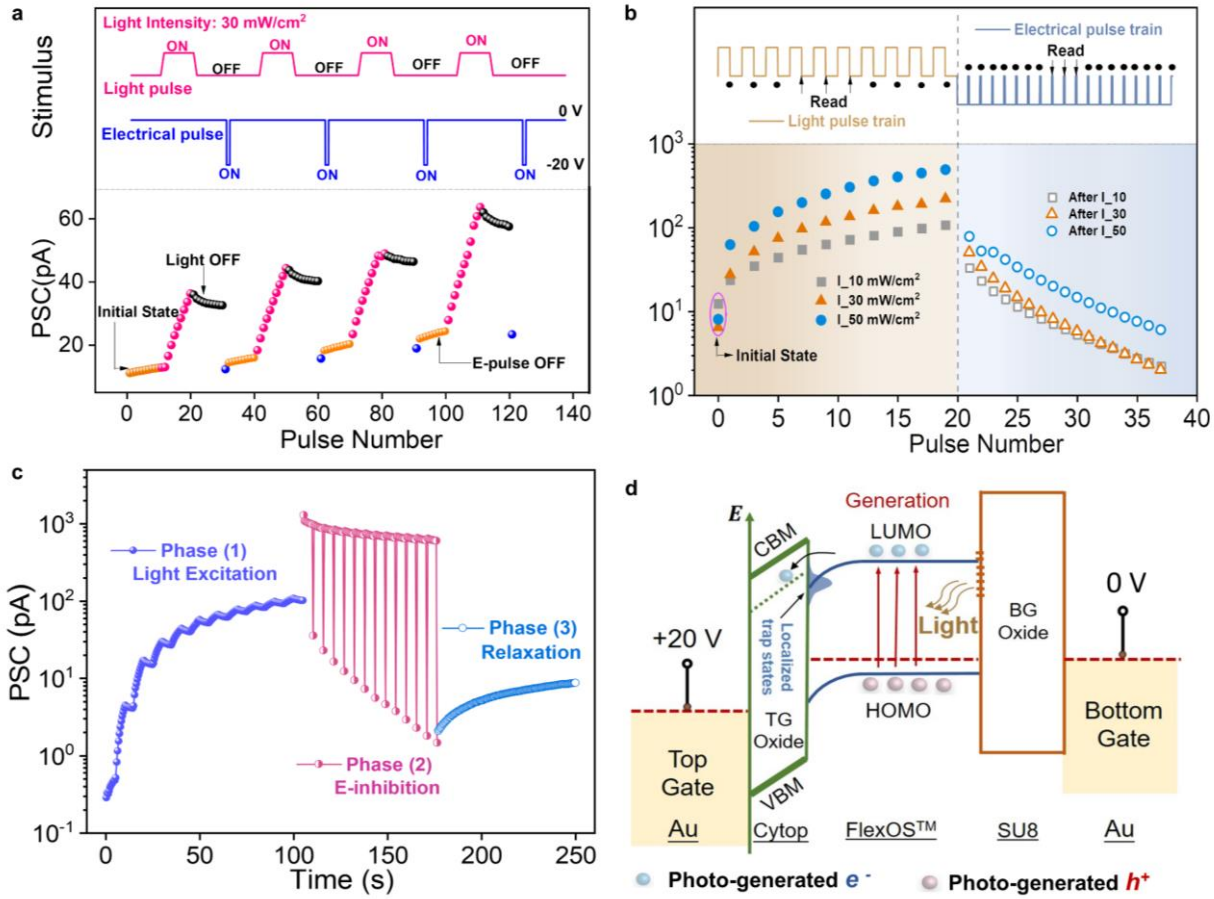

Figure 3. Optoelectronic-coupled performance of the transistor. (a) The "learning-forgetting-erasing" process of four cycles. (b) Long-term potentiation and depression characteristics of the device in weight update for visual neuromorphic computing. 10 consecutive optical spikes (pulse width = 5 s) with different intensities are applied for potentiation process, followed by several consecutive negative electrical spikes (−10 V, 0.5 s) for depression process. (c) The transient PSC diagram shows three phases of transistor current dynamics upon blue light (470 nm) illumination, which is respectively relevant to the learning-erasing-relaxing processes of visual system. (d) Indication of the detailed energy diagram for light excitation response mechanism.

Furthermore, we explore the device's photosensitivity in specific wavelengths other than white light to examine its feasibility in visible imaging scenarios. As depicted in **Figure** 3c, when the device is illuminated with blue light (470 nm), it exhibits similar self-regulation responses to both photonic potentiation and electrical depression compared to white light. The experimental setups for different phases of photo-electrical response are described in **Figures** S4a-c, corresponding

to phase (1), phase (2), and phase (3), respectively. Ten consecutive pulses of blue light (pulse width of 5 s and pulse interval of 5 s) result in a three-order-of-magnitude increase in PSC during phase (1), attributed to the photoconductive effect of the FlexOSTM material. Notably, a rapid facilitation with a tenfold change in PSC is observed after the first light pulse (5 s), demonstrating the high photo-response sensitivity. Subsequently, a clear inhibition plasticity is emulated by applying a series of electrical pulse stimuli (pulse amplitude of V_{BG} = −10 V, pulse width of 0.5 s, and pulse interval of 5 s) during phase (2). Upon removal of the electrical stimulus, a slight relaxation is observed in the PSC during phase (3), underscoring the unique non-volatility of the light-induced conductance response. Significantly, the total power consumption of our device is highly competitive with or even superior to previous approaches. The optical power consumption per device is approximately 3 nW (device size: W/L = 20/6 μm). Taking into account the tenfold change in PSC after the first light pulse of 5 s, the photo sensitivity (S_P) is estimated to be less than 15 nJ/decade. The S_P can be calculated using the following equation:

$$S_p = P \cdot \partial(t) \,/\, \partial(\lg(I_{DS})) \tag{2}$$

where P represents the light power density and t denotes the light stimulus time. The electrical power consumption per device is approximately 400 pW, which can be further reduced by decreasing the pulse voltage, making it comparable to the power consumption of a biological synapse (≈10 pW).[33] The bio-realistic light phototransistors can directly convert incident light of a wide range of intensities (brightness) and wavelengths (color) into analogue conductance modulation to engage in real-time adaptive learning in applications that necessitate perceiving and comprehending their surrounding environment. Additionally, the TIPS-pentacene-based device is expected to exhibit a broad response within the wavelength range of 380 nm to 740 nm, encompassing a visible spectrum of light. In particular, the device demonstrates a photo response to green light (525 nm) and red light (633 nm), although relatively weaker in comparison to the response observed for blue light, as can be seen in **Figure** S5. The transient PSC curves are also respectively associated with the learning-erasing-relaxation processes of the visual system. Light illumination with short wavelength induced a large

enhancement of PSC, which can reach about 10^2 pA at 470 nm, and 50 pA at 525 nm, while red light irradiation (633 nm) produced the weakest effect at 10 pA. These differences in responsivity to various incident light wavelengths enable the same optoelectronic synapse device to recognize patterns of multiple colors.[34,35]

The remarkable photo-sensitive excitatory behaviors observed in the device can be attributed to the utilization of TIPS-pentacene as the active material. The specific design of TIPS-pentacene with a narrow bandgap (~1.6 eV) enables high optical response across the entire perceptible wavelength spectrum (380 nm to 740 nm) of the human eye. Additionally, the stacked structure of the device, with the TIPS-pentacene channel layer sandwiched between the top Cytop and bottom SU-8 dielectric layers, contributes to its prominent photo-sensitivity. Both the Cytop and SU-8 dielectric layers possess good optical transparency within the wavelength range of interest, thus minimizing additional light absorption.[36,37] The observed photon-triggered synaptic characteristics can be attributed to the photogating effect, a phenomenon widely observed in various semiconductor materials.[38-43] Under visible light illumination with photon energy ($h\upsilon$) greater than 1.6 eV, photo-excitation occurs within the channel layer. This excitation leads to the generation of a large number of electron-hole (*e*-*h*) pairs as electrons are excited from the highest occupied molecular orbital (HOMO) to the lowest unoccupied molecular orbital (LUMO) in TIPS-pentacene. The electric field applied to the top gate (TG) facilitates the rapid separation of these photo-generated *e*-*h* pairs (**Figure** 3d). The photo-generated electrons are attracted to the OSC/Cytop interface under the influence of the applied V_{TG}. Subsequently, these electrons become trapped by the inherent local defect states within the bulk and/or at the interface between the TIPS-pentacene layer and the Cytop dielectric layer. This trapping process creates a negative electric field at the gate, inducing positive carriers in the active film and reducing the turn-on voltage. The capacitive coupling effect effectively screens the voltage applied to the TG electrode. Simultaneously, the photo-generated holes contribute to the photocurrent. These combined effects lead to a substantial increase in the overall channel current, resulting in the observed persistent photocurrent in the TIPS-pentacene layer (phase (1) - “memory process” in **Figure** 3c). The spatial separation of transported holes and trapped electrons reduces

recombination and substantially improves carrier lifetime. Upon cessation of the illumination, electron de-trapping occurs in the channel, leading to recombination with holes (**Figure** S6a) and subsequent decay of the PSC ("forgetting process"). Subsequently, applying an electrical pulse to the bottom gate triggers hole trapping by localized defect states within the bottom SU-8 dielectric layer (**Figure** S6b), resulting in a noticeable decrease in PSC (phase (2) - "memory erasing process" in **Figure** 3c). Removal of the electrical pulse allows for hole de-trapping and a slight recovery of PSC (phase (3) - "memory recovery process" in **Figure** 3c).

Leveraging the unique inherent dynamics of our neuronic device, we demonstrate the phenomenon of paired-pulse facilitation (PPF), which holds significant importance in neuroscience for deciphering temporal visual or auditory signals using a dual-pulse programming approach.[44,45] PPF refers to a synaptic event triggered by two consecutive optical pulses, wherein the peak of the LPSC triggered by the second pulse is distinctly larger than that of the first pulse, as shown in **Figure** 4a. The LPSC peak is measured after 6 s of illumination at a light intensity of 40 $mW \cdot cm^{-2}$ and a paired light pulse interval of 10 s. The PPF is further examined by varying the paired-pulse interval in order to calculate the PPF index (ΔG)

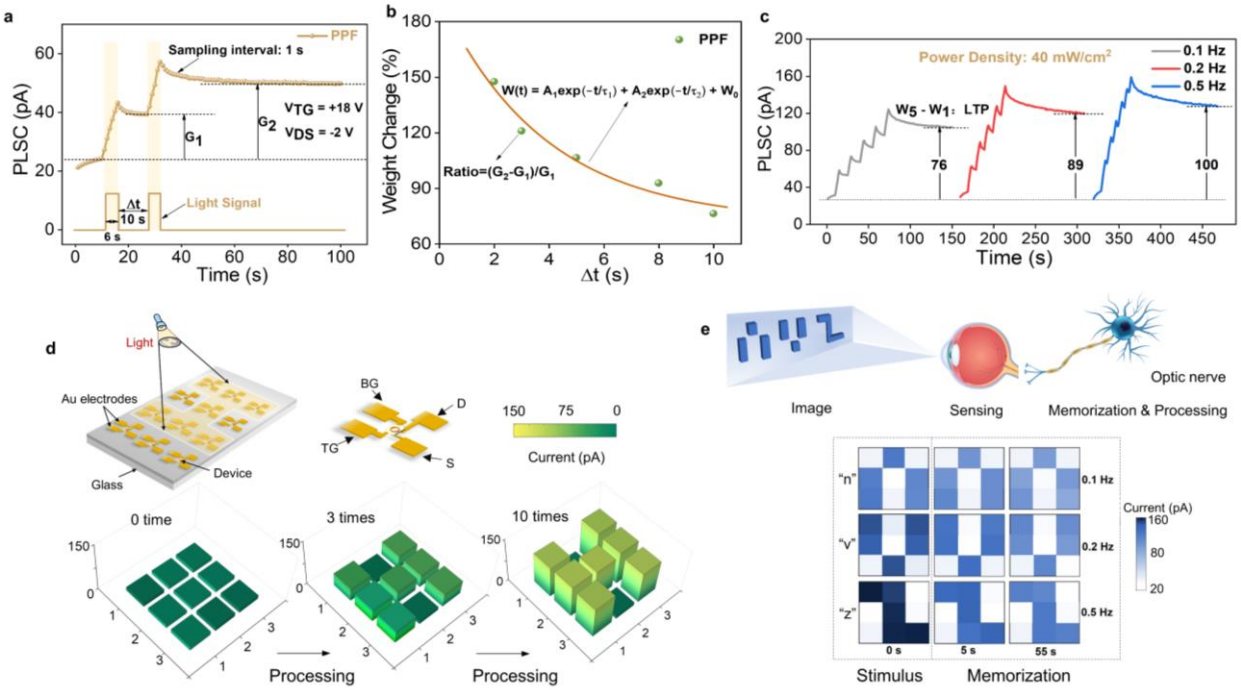

Figure 4. (a) Paired-pulse facilitation induction as a function of white light pulse duration. LPSC is triggered by two continuously applied optical pulses (40 mW·cm^{-2}, 6 s) with an interval of 10 s. G_1 and G_2 are the LPSC values at the end of the first and the second light pulse, respectively. (b) The variation of PPF index (ΔG) with the optical pulses interval (Δt) conforms to the double exponential time equation. (c) Frequency−dependent transient I−t profiles with increasing frequency under five successive light pulses, showing current dynamic with increasing pulse frequency. (d) Emulation of visual perception and memorization function in a 3 × 3 array. The times of pulses correspond to rehearsal. The array memorized the information 'H' more strongly for the increased times with rehearsal compared to that for the fewer times rehearsal (blue light with the intensity and duration of 40 mW·cm^{-2} and 5 s, respectively. (e) Visual information sensing-memory-processing system. The schematics of the input "N" "V", and "Z" letters in the shape of patterns and the corresponding encoded current maps and their dynamics. Memorization is enhanced with increasing frequency of light pulses. A V_{TGS} of +18 V and a V_{DS} of −2 V was used in all measurements.

according to $((G_2-G_1)/G_1) \times 100\%$, where G_1 and G_2 are the LPSC peaks corresponding to the first and second pulse, respectively. ΔG shows an inverse relationship with the paired-pulse interval and can be accurately fitted to a double exponential function (**Figure** 4b). Additionally, it is widely recognized in biology that synaptic responses exhibit intrinsic frequency selectivity, commonly referred to as spike-rate-dependent plasticity (SRDP). SRDP is a crucial form of synaptic plasticity that depends on the rate of external stimuli (pulse interval). In **Figure** 4c, we demonstrate the excitatory post-synaptic current (EPSC) in response to five consecutive light pulses, each with a duration of 6 seconds and an intensity of 40 mW·cm^{-2}. The spiking rate varies from 0.1 Hz to 0.5 Hz. We observe a clear increase in LPSC, which eventually reaches higher levels as the pulse frequency rises. Similar to human visual learning, our device exhibits enhanced memory

capacity when subjected to a high density of incident signals. Furthermore, in this study, we simulated advanced sensing-memory-processing capabilities, specifically in-sensor computing, by utilizing a 3 × 3 array of optoelectronic neurons. Our in-sensor computing system allows for real-time image acquisition and *in situ* image memory by manipulating light signals without the need for additional voltage regulation, as depicted in **Figure** 4d. Each device within the array represents one pixel, and a letter image with 3 × 3 pixels was input using the "H" shaped shadow mask. By applying various optical training pulses, we successfully fed the letter "H" into the system. The different colors in the image represent the different magnitudes of PSC. Initially, all neuronic devices were in a low current state I_0. Due to the long-term plasticity of our optoelectronic transistors, successive optical stimuli led to distinct conductance responses at different rehearsal times, all with the same duration of 5 seconds of illumination. The predefined image of "H" was clearly discernible by analyzing the contrast in PSC. With an increasing number of rehearsal times for external optical image stimulation, the LPSC of the visual pixels increased, resulting in more vivid and clear memorized images. Notably, the conductance response difference between the 1st and the 10th rehearsal reached approximately 100 pA after 10 learning iterations. To demonstrate the visual memories resulting from different training rates, we presented three letters, namely "N," "V," and "Z," to the array with varying stimulus rates. It was observed that the contrast of the images gradually increased with the frequency of rehearsals, as depicted in the stimulus panel in **Figure** 4e. Furthermore, the letter image, represented by the drain current value, remained distinctly visible even after a relaxation time of 55 s, showcasing the long-term memory plasticity akin to the human visual system (memorization panels in **Figure** 4e). Our AOEND arrays hold promising potential as fundamental building blocks for future bionic eyes. Additionally, high device integration density is critical for artificial visual systems to realize system miniaturization and high resolution. Our reproducible and reliable device offers outstanding advantage in this regard as well. The maximum pixel density of a robust array can reach up to 10^4 mm^{-2} without considering the peripheral circuits, which is comparable to the latest artificial vision chips based on MoS_2 devices.[46]

3. Conclusion

In summary, we have successfully presented an all-organic optoelectronic neuronic device that effectively emulates human visual perception and memory functions, offering high photo-sensitivity (15 nJ/dec) and low light power consumption (~3 nW). The remarkable performance of our device can be attributed to two key factors: (i) the TIPS-pentacene OSC layer, which exhibits a tunable narrow bandgap and enables efficient response to the entire range of wavelengths perceivable by human eyes, resembling the behavior of neurons, and (ii) the unique design of the device architecture, where the OSC layer is sandwiched between top and bottom wide-bandgap dielectric layers that do not absorb the targeted light wavelength. Additionally, the resultant phototransistor array is compatible with industrial manufacturing processes and possesses remarkable flexibility. This study opens up exciting opportunities in the realm of efficient and flexible neuromorphic vision systems at edge terminals, where power efficiency and adaptability are paramount. To the best of our knowledge, our device represents a promising candidate for achieving human-like visual networks with low power consumption and versatility.

4. Methods

Device fabrication

The Corbino and interdigitated OTFTs employ top gate bottom contact (TGBC) architecture. Au (~50 nm) layer was first deposited on the PET flexible substrate by sputtering and patterned using UV photolithography and wet etching to form the bottom gate electrode. After that, SU-8 (~380 nm) bottom dielectric layer was spin-coated. Then another Au (50 nm) layer was sputter coated and patterned using same photolithography and wet etching process to generate drain and source electrodes. Afterwards, the truFLEX® organic semiconductor (OSC) solution was spin-coated at 500 rpm for 10 s followed by 1000 rpm for 60 s and then a further bake at 100°C for 60 s to get a 50 nm thick OSC film. Subsequently, top AGC Cytop dielectric layer (~250 nm) was spin-coated. Finally, Au (50 nm) top gate electrode was formed using the

same process as above-mentioned. The unwanted areas of OSC and Cytop dielectric were removed by oxygen reactive-ion etching (RIE) using the gate metal as a hard-mask. All the layer thicknesses were measured through high-resolution cross-sectional transmission electron microscopy (HRTEM) images.

Device characterization

The electrical and optoelectronic measurements of the dual-gated synaptic transistor were performed in a probe station connected to a Keithley 4200-SCS semiconductor parameter analyzer and a Keysight B1530 with arbitrary waveform generator at atmosphere and room temperature. Light spike pulses were provided by the Sugar CUBE ultra LED broadband white light source for device optical characterization measurements. Blue-light pulse with power density of 2.5 $mW \cdot cm^{-2}$ is illuminated to the device through application of specific light filter. The light intensity was measured with a power meter (daystar meter). If not specified, the channel currents were read out at V_{TG} =+18 V and V_{DS} =−2 V. DC current-voltage (*I*−*V*) measurements were carried out at a sweeping rate of 0.01 V/s. The test devices in an array have the dimension area of W×L = 20×6 μm^2.

Acknowledgements

We thank D. Ang for the laboratory of device characterization. This work is supported by National Research Foundation Competitive Research Programs (NRF-CRP24-2020-0002), Beijing Natural Science Foundation (Grant No. Z210006), National Natural Science Foundation of China (Grant No. 92064006), the Hong Kong Research Grant Council-Early Career Scheme (Grant No. 27206321), National Natural Science Foundation of China-Excellent Young Scientists Fund (Hong Kong and Macau) (Grant No. 62122004).

Author information

Correspondence to Haizhong Zhang and Xin Ju.

Author contributions

H.Z.Z. conceived the idea and lead the project, X.J. proposed the collaboration and performed the measurement, L.R.F., Z. L. fabricated the devices, H.Z.Z., X.J., M.M.Z., T.Y.L., R.S.W., S.H.W. carried out the analysis, D.Z.C., K.S.Y., L.F.S., Z.R.W., Q.Y.W. designed the experiments. All authors contributed to the preparation of the manuscript.

Conflicts of interest

The authors declare no competing financial interest.

Supplementary information

Supplementary Figs. S1-S6.

References

(1) Gu, L.; Poddar, S.; Lin, Y.; Long, Z.; Zhang, D.; Zhang, Q.; Shu, L.; Qiu, X.; Kam, M.; Javey, A.; Fan, Z.-Y. A Biomimetic Eye with a Hemispherical Perovskite Nanowire Array Retina. *Nature* **2020**, *581*, 278−282.

(2) Zhang, K.; Jung, Y. H.; Mikael, S.; Seo, J. H.; Kim, M.; Mi, H. Y.; Zhou, H.; Xia, Z. Y.; Zhou, W. D.; Gong, S. Q.; Ma, Z. Q. Origami silicon optoelectronics for hemispherical electronic eye systems. *Nat. Commun.* **2017**, *8*, 1782.

(3) Choi, C.; Choi, M. K.; Liu, S.; Kim, M. M. S.; Park, O. K.; Im, C.; Kim, J.; Qin, X.; Lee, G. J.; Cho, K. W.; Kim, M. M. S.; Joh, E.; Lee, J.; Son, D.; Kwon, S. H.; Jeon, N. L.; Song, Y. M.; Lu, N.; Kim, D. H. Human Eye-Inspired Soft Optoelectronic Device Using High-Density MoS_2-Graphene Curved Image Sensor Array. *Nat. Commun.* **2017**, *8*, 1664.

(4) Liao, F.; Zhou, Z.; Kim, B. J.; Chen, J.; Wang, J.; Wan, T.; Zhou, Y.; Hoang, A. T.; Wang, C.; Kang, J.; Ahn, J.-H.; Chai, Y. Bioinspired In-sensor Visual Adaptation for Accurate Perception. *Nat. Electron.* **2022**, *5*, 84−91.

(5) Mennel, L.; Symonowicz, J.; Wachter, S.; Polyushkin, D. K.; Molina-Mendoza, A. J.; Mueller, T. Ultrafast machine vision with 2D material neural network image sensors. *Nature* **2020**, *579*, 62−66.

(6) Song, Y. M.; Xie, Y.; Malyarchuk, V.; Xiao, J.; Jung, I.; Choi, K.- J.; Liu, Z.; Park, H.; Lu, C.; Kim, R.-H.; Li, R.; Crozier, K. B.; Huang, Y.; Rogers, J. A. Digital Cameras with Designs Inspired by the Arthropod Eye. *Nature* **2013**, *497*, 95−99.

(7) Lee, G. J.; Choi, C.; Kim, D.-H.; Song, Y. M. Bioinspired Artificial Eyes: Optic Components, Digital Cameras, and Visual Prostheses. *Adv. Funct. Mater.* **2018**, *28*, 1705202.

(8) Wan, C.; Cai, P.; Wang, M.; Qian, Y.; Huang, W.; Chen, X. Artificial Sensory Memory. *Adv. Mater.* **2019**, *32*, 1902434.

(9) Zhou, F.; Zhou, Z.; Chen, J.; Choy, T. H.; Wang, J.; Zhang, N.; Lin, Z.; Yu, S.; Kang, J.; Wong, H. S. P.; Chai, Y. Optoelectronic Resistive Random Access Memory for Neuromorphic Vision Sensors. *Nat. Nanotechnol.* **2019**, *14*, 776−782.

(10) Zhu, Q. B.; Li, B.; Yang, D. D.; Liu, C.; Feng, S.; Chen, M. L.; Sun, Y.; Tian, Y. N.; Su, X.; Wang, X. M.; Qiu, S.; Li, Q. W.; Li, X. M.; Zeng, H. B.; Cheng, H. M.; Sun, D. M. A Flexible Ultrasensitive Optoelectronic Sensor Array for Neuromorphic Vision Systems. *Nat. Commun.* **2021**, *12*, 1−7.

(11) Wang, C.-Y.; Liang, S.-J.; Wang, S.; Wang, P.; Li, Z a; Wang, Z.; Gao, A.; Pan, C.; Liu, C.; Liu, J.; Yang, H.; Liu, X.; Song, W.; Wang, C.; Cheng, B.; Wang, X.; Chen, K.; Wang, Z.; Watanabe, K.; Taniguchi, T.; Yang, J. J.; Miao, F. Gate-tunable van der Waals heterostructure for reconfigurable neural network vision sensor. *Sci. Adv.* **2020**, *6*, eaba6173.

(12) Sun, L.; Wang, Z.; Jiang, J.; Kim, Y.; Joo, B.; Zheng, S.; Lee, S.; Yu, W. J.; Kong, B. S.; Yang, H. In-Sensor Reservoir Computing for Language Learning Via Two-Dimensional Memristors. *Sci. Adv.* **2021**, *7*, eabg1455.

(13) Hou, X.; Liu, C. S.; Ding, Y.; Liu, L.; Wang, S. Y.; Zhou, P. A Logic-Memory Transistor with the Integration of Visible Information Sensing-Memory-Processing. *Adv. Sci.* **2020**, *7*, 2002072.

(14) Tu, L.; Cao, R.; Wang, X.; Chen, Y.; Wu, S.; Wang, F.; Wang, Z.; Shen, H.; Lin, T.; Zhou, P.; Meng, X.; Hu, W.; Liu, Q.; Wang, J.; Liu, M.; Chu, J. Ultrasensitive Negative Capacitance Phototransistors. *Nat. Commun.* **2020**, *11*, 101.

(15) Kwon, S. M.; Cho, S. W.; Kim, M.; Heo, J. S.; Kim, Y.-H.; Park, S. K. Environment-Adaptable Artificial Visual Perception Behaviors Using a Light-Adjustable Optoelectronic Neuromorphic Device Array. *Adv. Mater.* **2019**, *31*, 1906433.

(16) Feng, G.; Jiang, J.; Li, Y.; Xie, D.; Tian, B.; Wan, Q. Flexible Vertical Photogating Transistor Network with an Ultrashort Channel for In-Sensor Visual Nociceptor. *Adv. Funct. Mater.* **2021**, *31*, 2104327.

(17) Yu, J. J.; Liang, L. Y.; Hu, L. X.; Duan, H. X.; Wu, W. H.; Zhang, H. L.; Gao, J. H.; Zhuge, F.; Chang, T. C.; Cao, H. T. Optoelectronic Neuromorphic Thin-film Transistors Capable of Selective Attention and with Ultra-low Power

Dissipation. *Nano Energy* **2019**, *62*, 772−780.

(18) Sun, J.; Oh, S.; Choi, Y.; Seo, S.; Oh, M. J.; Lee, M.; Lee, W. B.; Yoo, P. J.; Cho, J. H.; Park, J.-H. Optoelectronic Synapse Based on IGZO-Alkylated Graphene Oxide Hybrid Structure. *Adv. Funct. Mater.* **2018**, *28*, 1804397.

(19) Tan, H.; Ni, Z.; Peng, W.; Du, S.; Liu, X.; Zhao, S.; Li, W.; Ye, Z.; Xu, M.; Xu, Y.; Pi, X.; Yang, D. Broadband Optoelectronic Synaptic Devices Based on Silicon Nanocrystals for Neuromorphic Computing. *Nano Energy* **2018**, *52*, 422−430.

(20) Yang, L.; Singh, M.; Shen, S. W.; Chih, K. Y.; Liu, S. W.; Wu, C. I.; Chu, C. W.; Lin, H. W. Transparent and Flexible Inorganic Perovskite Photonic Artificial Synapses with Dual-Mode Operation. *Adv. Funct. Mater.* **2021**, *31*, 2008259.

(21) Zhu, X.; Lu, W. D. Optogenetics-Inspired Tunable Synaptic Functions in Memristors. *ACS Nano* **2018**, *12*, 1242−1249.

(22) He, H.-K.; Yang, R.; Zhou, W.; Huang, H.-M.; Xiong, J.; Gan, L.; Zhai, T.-Y.; Guo, X. Photonic Potentiation and Electric Habituation in Ultrathin Memristive Synapses Based on Monolayer MoS_2. *Small* **2018**, *14*, 1800079.

(23) John, R. A.; Liu, F.; Chien, N. A.; Kulkarni, M. R.; Zhu, C.; Fu, Q.; Basu, A.; Liu, Z.; Mathews, N. Synergistic Gating of Electro-Iono-Photoactive 2D Chalcogenide Neuristors: Coexistence of Hebbian and Homeostatic Synaptic Metaplasticity. *Adv. Mater.* **2018**, *30*, 1800220.

(24) Yan, J.-M.; Ying, J.-S.; Yan, M.-Y.; Wang, Z.-C.; Li, S.-S.; Chen, T.-W.; Gao, G.-Y.; Liao, F.; Luo, H.-S.; Zhang, T.; Chai, Y.; Zheng, R.-K. Optoelectronic Coincidence Detection with Two-Dimensional Bi_2O_2Se Ferroelectric Field-Effect Transistors. *Adv. Funct. Mater.* **2021**, *31*, 2103982.

(25) Wang, H.; Zhao, Q.; Ni, Z.; Li, Q.; Liu, H.; Yang, Y.; Wang, L.; Ran, Y.; Guo, Y.; Hu, W.; Liu, Y. A. Ferroelectric/Electrochemical Modulated Organic Synapse for Ultraflexible, Artificial Visual-Perception System. *Adv. Mater.* **2018**, *30*, 1803961.

(26) Zhang, J.; Shi, Q.; Wang, R.; Zhang, X.; Li, L.; Zhang, J.; Tian, L.; Xiong, L.; Huang, J. Spectrum-Dependent Photonic Synapses Based on 2D Imine Polymers for Power-Efficient Neuromorphic Computing. *InfoMater.* **2021**, *3*, 904.

(27) Lago, N.; Buonomo, M.; Imran, S.; Bertani, R.; Wrachien, N.; Bortolozzi, M.; Pedersen, M. G.; Cester, A. TIPS-pentacene as biocompatible material for solution processed high-performance electronics operating in water. *IEEE Electron Device Lett.* **2018**, *39*, 1401−1404.

(28) Griffith, O. L.; Anthony, J. E.; Jones, A. G.; Lichtenberger, D. L. Electronic properties of pentacene versus triisopropylsilylethynyl-substituted pentacene: Environment-dependent effects of the silyl substituent. *J. Am. Chem. Soc.* **2009**, *132*, 580−586.

(29) Feng, P.; Xu, W.; Yang, Y.; Wan, X.; Shi, Y.; Wan, Q.; Zhao, J.; Cui, Z. Printed Neuromorphic Devices Based on Printed Carbon Nanotube Thin-Film Transistors. *Adv. Funct. Mater.* **2017**, *27* (5), 1604447.

(30) Du, C.; Ma, W.; Chang, T.; Sheridan, P.; Lu, W. D. Biorealistic implementation of synaptic functions with oxide memristors through internal ionic dynamics. *Adv. Funct. Mater.* **2015**, *25* (27), 4290− 4299.

(31) Zhang, H.; Ju, X.; Yew, K. S.; Ang, D. S. Implementation of Simple but Powerful Trilayer Oxide-Based Artificial Synapses with A Tailored Bio-Synapse-Like Structure. *ACS Appl. Mater. Interfaces* **2020**, *12*, 1036−1045.

(32) Hou, Y.-X.; Li, Y.; Zhang, Z.-C.; Li, J.-Q.; Qi, D.-H.; Chen, X.- D.; Wang, J.-J.; Yao, B.-W.; Yu, M.-X.; Lu, T.-B.; Zhang, J. Large-Scale and Flexible Optical Synapses for Neuromorphic Computing and Integrated Visible Information Sensing Memory Processing. *ACS Nano* **2021**, *15*, 1497−1508.

(33) Wang, Y.; Wang, R.; Xu, X. Neural energy supply-consumption properties based on Hodgkin-Huxley model. *Neural Plasticity*, **2017**.

(34) Zhang, J.; Lu, Y.; Dai, S.; Wang, R.; Hao, D.; Zhang, S.; Xiong, L.; Huang, J. Retina-inspired organic heterojunction-based optoelectronic synapses for artificial visual systems. *Research* **2021**, 1

(35) Seo, S.; Jo, S.-H.; Kim, S.; Shim, J.; Oh, S.; Kim, J.-H.; Heo, K.; Choi, J.-W.; Choi, C.; Oh, S.; et al. Artificial optic-

neural synapse for colored and color-mixed pattern recognition. *Nat. Commun.* **2018**, 9 (1), 1−8.

(36) Takahashi, T.; Zhang, H.; Kawakami, R.; Yarinome, K.; Agetsuma, M.; Nabekura, J.; Otomo, L.; Nemoto, T. PEO-CYTOP fluoropolymer nanosheets as a novel open-skull window for imaging of the living mouse brain. *Iscience* **2020**, *23*, 101579.

(37) Chen, Z.; Lee, J. B. Biocompatibility of su-8 and its biomedical device applications. *Micromachines* **2021**, *12*, 794.

(38) Hou, Y.; Wang, L.; Zou, X.; Wan, D.; Liu, C.; Li, G.; Liu, X.; Liu, Y.; Jiang, C.; Ho, J. C.; Liao, L. Substantially Improving Device Performance of All-Inorganic Perovskite-Based Phototransistors via Indium Tin Oxide Nanowire Incorporation. *Small* **2020**, *16*, 1905609.

(39) Wang, Y.; Zhu, Y.; Li, Y.; Zhang, Y.; Yang, D.; Pi, X. Dual-Modal Optoelectronic Synaptic Devices with Versatile Synaptic Plasticity. *Adv. Funct. Mater.* **2022**, *32*, 2107973.

(40) Fang, H.; Hu, W. Photogating in Low Dimensional Photodetectors. *Adv. Sci.* **2017**, *4*, 1700323.

(41) Feng, G.; Jiang, J.; Li, Y.; Xie, D.; Tian, B.; Wan, Q. Flexible Vertical Photogating Transistor Network with an Ultrashort Channel for In-Sensor Visual Nociceptor. *Adv. Funct. Mater.* **2021**, *31*, 2104327.

(42) Luo, P.; Zhuge, F. W.; Wang, F. K.; Lian, L. Y.; Liu, K. L.; Zhang, J. B.; Zhai, T. Y. PbSe Quantum Dots Sensitized High-Mobility Bi_2O_2Se Nanosheets for High-Performance and Broadband Photodetection beyond 2 μm. *ACS Nano* **2019**, *13*, 9028−9037.

(43) Islam, M. M.; Krishnaprasad, A.; Dev, D.; Martinez-Martinez, R.; Okonkwo, V.; Wu, B.; Han, S. S.; Bae, T.-S.; Chung, H.-S.; Touma, J.; Jung, Y.; Roy, T. Multiwavelength Optoelectronic Synapse with 2D Materials for Mixed-Color Pattern Recognition. *ACS Nano* **2022**, *16*, 10188−10198.

(44) Chen, C.; He, Y.; Mao, H.; Zhu, L.; Wang, X.; Zhu, Y.; Zhu, Y.; Shi, Y. A Photoelectric Spiking Neuron for Visual Depth Perception. *Adv. Mater.* **2022**, *34*, 2201895.

(45) He, K.; Liu, Y.; Yu, J.; Guo, X.; Wang, M.; Zhang, L.; Wan, C.; Wang, T.; Zhou, C.; Chen, X. Artificial Neural Pathway Based on a Memristor Synapse for Optically Mediated Motion Learning. *ACS Nano* **2022**, *16*, 9691−9700.

(46) Ma, S.; Wu, T.; Chen, X.; et al. A 619-pixel machine vision enhancement chip based on two-dimensional semiconductors. *Sci. Adv.* **2022** *8*, eabn9328.